Modelling the hysteretic characteristics of a magnetorheological fluid damper

En Rong Wang[1,2]*, **Xiao Qing Ma**[2], **S Rakhela**[2] and **C Y Su**[2]
[1]Faculty of Electrical and Electronic Engineering, Nanjing Normal University, Nanjing, People's Republic of China
[2]Department of Mechanical Engineering, Concordia University, Montreal, Canada

Abstract: A generalized model is proposed to characterize the biviscous hysteretic force characteristics of a magnetorheological (MR) fluid damper using symmetric and asymmetric sigmoid functions on the basis of a fundamental force generation mechanism, observed qualitative trends and measured data under a wide range of control and excitation conditions. Extensive laboratory measurements were performed to characterize the hysteretic force properties of an MR damper under a wide range of magnitudes of control current and excitation conditions (frequency and stroke). The global model is realized upon formulation and integration of component functions describing the preyield hysteresis, saturated hysteresis loop, linear rise and current-induced rise. The validity of the proposed model is demonstrated by comparing the simulation results with measured data in terms of hysteretic force–displacement and force–velocity characteristics under a wide range of test conditions. The results revealed reasonably good agreement between the measured data and model results, irrespective of the test conditions considered. The results of the study suggest that the proposed model could be effectively applied for characterizing the damper hysteresis and for development of an optimal controller for implementation in vehicular suspension applications.

Keywords: magnetorheological fluid damper, hysteresis, hysteresis model, force limiting, experimental force–velocity characterization

NOTATION

a_m	excitation stroke (m)
a_0	positive constant associated with the hysteresis slope coefficient α
a_1	positive constant adjusting the rising rate of the exponent v_m [(m/s)$^{-1}$]
a_2	positive constant associated with the control current gain c_i (A^{-1})
a_3	positive constant associated with the zero-force velocity intercept v_h (A^{-1})
a_4	positive constant associated with the linear rise coefficient k_v [(m/s)$^{-1}$]
c_e, $c_e(v_m)$	excitation condition gain
c_i, $c_i(i)$	control current gain
$c_v(v)$	high-velocity damping coefficient
ER	electrorheological
f	instantaneous force (N)
$f(v+v_h)$	force in a general hysteresis loop (N)
f_h	zero-velocity force intercept (N)
f_m	maximum force developed by the damper (N)
$f_s(v+v_h)$	force in a saturated hysteresis loop in the absence of a linear rise (N)
f_t	transition force (N)
f_0	seal friction force (N)
i	current (A)
I_0	arbitrary constant associated with the control current gain c_i (A)
I_1	arbitrary constant associated with the zero-force velocity intercept v_h (A)
k_v	linear rise coefficient
k_0	positive constant associated with the hysteresis slope coefficient α
k_1	positive constant associated with the linear rise coefficeint k_v
k_2	positive constant associated with the control current gain c_i
k_3, k_4	positive constant associated with the zero-force velocity intercept v_h
MR	magnetorheological
v, $\dot{x}$	instantaneous piston velocity (m/s)
v_h	zero-force velocity intercept (m/s)

The MS was received on 3 May 2002 and was accepted after revision for publication on 7 February 2003.
* *Corresponding author: Department of Mechanical Engineering, Concordia University, 1455 de Maisonneuwe Blvd West, Montreal, Quebec, Canada H3G 1M8.*

v_m	maximum velocity of the damper piston (m/s)
v_t	transition velocity (m/s)
x	instantaneous piston displacement (m)
$\ddot{x}$, dv/dt	instantaneous piston acceleration (m/s^2)
α	hysteresis slope coefficient
β_h	high-velocity slope (N s/m)
β_l	low-velocity slope (N s/m)
ω	excitation frequency (rad/s)

1 INTRODUCTION

A wide range of magnetorheological (MR) fluid-based dampers are currently being explored for their potential implementation in various systems, such as vibration control devices and vehicle suspension. A number of analytical and experimental studies have clearly established superior potential performance benefits of MR dampers in vehicle applications in relation to conventional hydraulic dampers [**1**–**3**]. The MR dampers offer high viscous damping corresponding to low velocities in the preyield condition, while the post-yield saturation corresponding to high velocities can be characterized by a considerably lower viscous damping coefficient. The requirement of adequate ride, road-holding, handling and directional control stability performance of road vehicles entails variable damping [**4**] which could be achieved with MR dampers with only minimal power consumption. The MR damper is considered to be a continuously controlled semi-active damper, since it offers only variable damping force with minimal power requirement, unlike a fully active suspension which could add or remove energy depending upon the demand with the help of an elaborate power supply. The semi-actively controlled MR fluid dampers offer rapid variation in damping properties in a reliable fail-safe manner, since they continue to provide adequate damping, in a passive manner, in the event of a control hardware malfunction [**5**]. Although a vast number of semi-active variable damping concepts based upon hydraulic flow modulation and electrorheological (ER) fluids have been developed, clear advantages of the MR fluid dampers have been established, such as significantly higher yield stress and a wider operating temperature range [**5**–**7**].

Owing to the rheology of the MR fluid in terms of its shear stress–strain rate behaviour, the damper exhibits highly non-linear variations in damping force, attributed to the hysteresis and force-limiting properties of the fluid as functions of the intensity of the applied magnetic field, and displacement and velocity of the piston. The development of an effective controller for realizing desirable variations in damping requires accurate characterization of the hysteretic force–velocity characteristics of the MR damper in the preyield condition, and force saturation in the post-yield condition. In view of the highly non-linear properties of MR dampers, considerable attempts are being made to study their dynamic behaviour for model synthesis and for developing effective control algorithms [**5**–**9**]. Dyke *et al.* [**10**] proposed a damper model on the basis of the Bouc–Wen hysteresis model. The model, however, poses inherent difficulties in predicting essential parameters and in realizing control systems for desired tracking control performance. The Bingham plastic model which has been proposed assumes rigid material behaviour in the preyield, while the shear flow in the post-yield is characterized by a viscous damping coefficient [**7**]. Assuming the material to be plastic in both pre- and post-yield conditions, Stanway *et al.* [**11**] proposed a non-linear model, where the preyield force is characterized by a considerably high viscous damping. On the basis of this model, Wereley *et al.* [**7**] proposed a non-linear hysteretic bilinear model by fitting the force–velocity characteristics using four parameters: pre- and post-yield viscous damping coefficients, yield force and zero-force velocity intercept. The above models, however, do not include the effects of continually varying control current. Moreover, the hysteretic damping force generated by an MR damper depends not only upon the intensity of the magnetic field but also upon the excitation frequency and amplitude of the damper motion. This dependence of the hysteretic force on the nature of excitation has not yet been accurately characterized.

In this study, a series of laboratory tests have been performed to characterize the dependence of the hysteretic damping force of an MR damper on the excitation frequency and stroke and the control current. The measured data are used to synthesize a generalized model of the MR damper on the basis of a symmetric sigmoid function. The effectiveness of the proposed hysteretic model is demonstrated by comparing the simulation results with the measured data over a wide range of excitation parameters and magnitudes of control current. The proposed model could thus be used for control algorithm development and for assessment of the vibration attenuation performance of a semi-actively controlled MR damper.

2 TEST METHODOLOGY

An MR damper, schematically shown in Fig. 1, is considered for modelling of its hysteretic force–velocity characteristics. The damper consists of a nitrogen-charged accumulator and two MR fluid chambers separated by a piston with orifices and coils. The variations in viscous and shear properties of the fluid, caused by the applied magnetic field, cause variations in the damping force. A d.c. current, limited to 2 A, serves as the command signal as well as the input for the coils.

The force–velocity and force–displacement characteristics of the test MR damper are measured in the

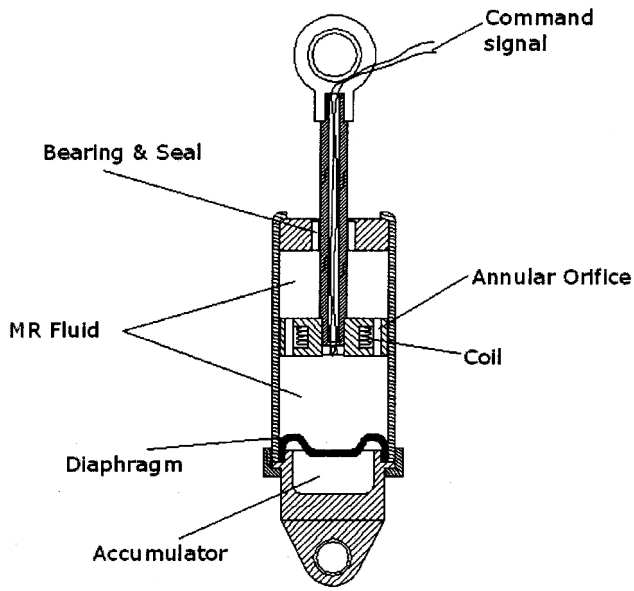

Fig. 1 Schematic configuration of the test MR damper

laboratory to characterize the damper hysteresis over a range of excitations. The damper is installed on an electrohydraulic vibration exciter between the exciter and a fixed inertial frame through a force transducer. Position (LVDT) and velocity (LVT) sensors are installed on the exciter to measure the instantaneous position and velocity of the damper piston. The damper is subject to harmonic displacement excitations of different constant amplitudes at selected discrete frequencies. The force, velocity and displacement data, acquired through a data acquisition board, are used to provide on-line displays of hysteretic force–velocity characteristics. A dual regulated d.c. power supply is used to supply the control current to the damper. A thermocouple is also mounted on the damper body to monitor the damper temperature in order to ensure the data were obtained within a defined temperature range ($30 \pm 10\,^{\circ}\mathrm{C}$).

The hysteretic force–velocity characteristics of the MR fluid damper are measured under sinusoidal displacement excitations in the 0–15 Hz frequency range, which is considered to represent the range of predominant vehicular ride motions along the vertical axis [**4**]. The tests are performed with constant magnitudes of displacement, ranging from 2.5 to 18.75 mm, and control currents to the coil in the range 0–1.5 A. A total of 245 tests were performed, corresponding to different combinations of frequency (0.1, 0.5, 1.5, 2.5, 5.0, 7.5, 10.0, 12.5 and 15.0 Hz), stroke (2.5, 6.35, 12.5 and 18.75 mm) and control current (0.0, 0.25, 0.5, 0.75, 1.0, 1.25 and 1.5 A). The amplitudes of displacement excitations at higher frequencies were limited to lower values to ensure damper operation within safe velocity limits.

2.1 Force–velocity and force–displacement characteristics

As an example, Fig. 2 illustrates the measured force, velocity and displacement time histories together with force–displacement (f–d) and force–velocity (f–v) characteristics as a function of the control current, i, under 6.25 mm displacement excitation at 2.5 Hz. It should be noted that the force–displacement loops in Fig. 2b follow a clockwise path with increasing time, while the force–velocity loops in Fig. 2c follow a counterclockwise path with increasing time. The results shown in Figs 2b and c clearly show the strong dependence of damper hysteresis in the preyield condition on the applied current. The f–v characteristics further show the post-yield force-limiting behaviour which also relies strongly on the applied current. Such non-linear damper properties are further dependent upon the excitation frequency and amplitude, as evident from Fig. 3. Considering that the performance characteristics of suspension dampers are mainly evaluated in terms of f–v properties, further data analysis and model synthesis are limited to these data alone.

The data acquired under extremely low frequency (0.083 Hz) and amplitude (2.5 mm) were used to evaluate the contribution of seal friction alone. The results (not shown) revealed negligible seal friction in relation to the fluid hysteresis.

The essential dynamic behaviour of the MR damper required for model synthesis can be deduced from the f–d and f–v characteristics shown in Figs 2 and 3 and summarized below:

1. *Incremental feature.* The f–v characteristics of MR dampers can be generally represented as symmetric bi-non-linear curves with significant hysteresis at lower velocities (preyield), followed by a linearly increasing force at higher velocities (post-yield). A force-limiting behaviour is also evident during transition between low and high velocity responses. This behaviour is also evident in the f–v characteristics of typical hydraulic dampers with low-speed bleed flows and high-speed blow-off valves [**12**]. The damping force may thus be characterized as an incremental function of velocity in the pre- and post-yield conditions.
2. *Passive behaviour.* The MR damper exhibits an almost viscous property when zero control current is applied (passive property), as evident from the near-elliptical f–d curve and near-linear f–v curve with relatively small hysteresis (Figs 2b and c).
3. *Controllability.* The damping force increases considerably with the magnitude of the control current. The measured yield force (the force developed at the onset of post-yield saturation) corresponding to either $\mathrm{d}v/\mathrm{d}t < 0$ (upper f–v curve) or $\mathrm{d}v/\mathrm{d}t > 0$ (lower f–v curve) can be observed with increasing control

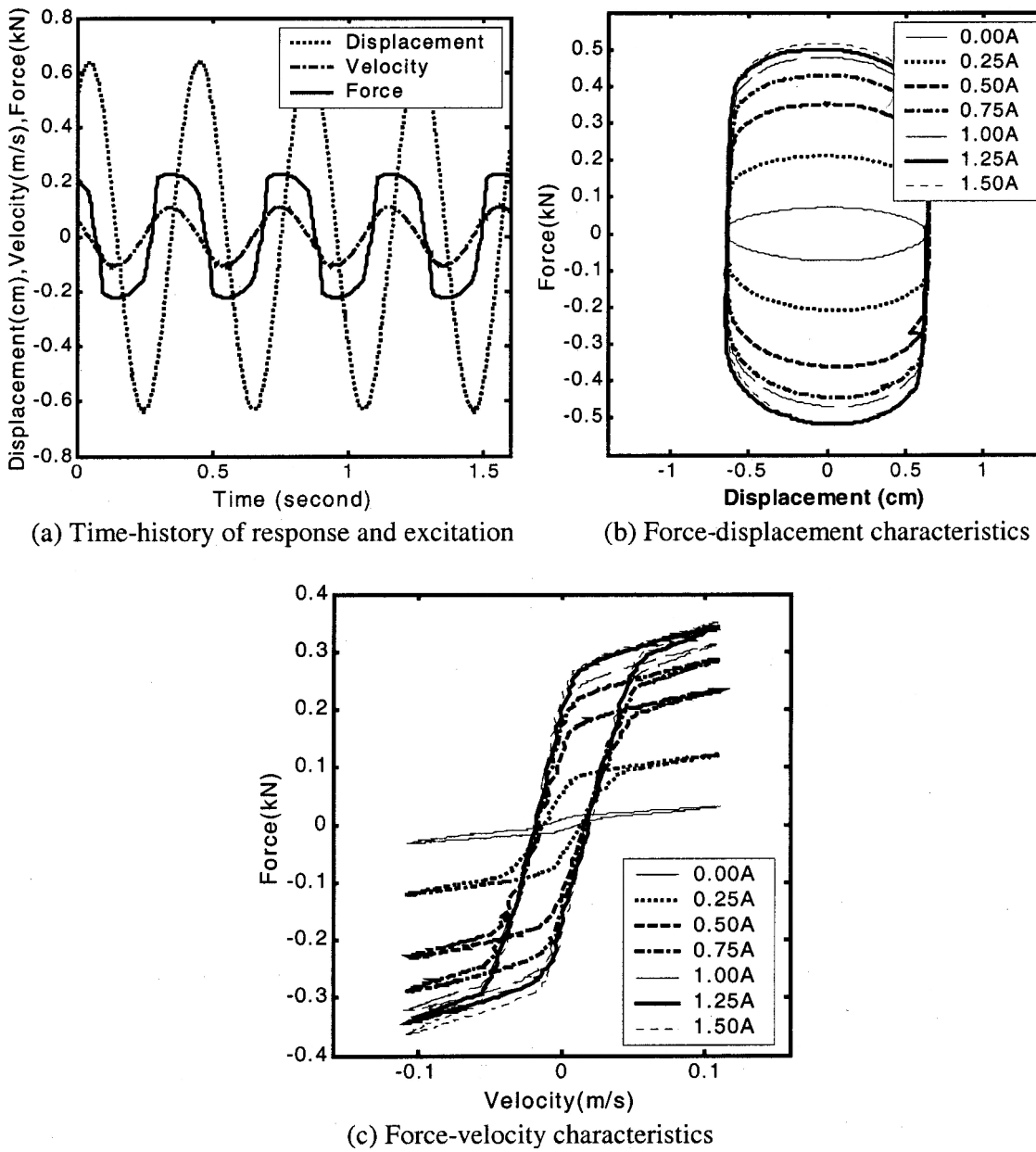

Fig. 2 Measured damper responses as functions of applied current

currents. The rate of increase in force magnitude is approximately linear under lower current levels (<0.5 A), which tends gradually to decrease under higher values of applied current (0.5–1.25 A). A further increase in current (>1.25 A) yields saturation of the damping force.

4. *Hysteretic phenomenon.* The damper hysteresis progresses along a counterclockwise path with increasing time (Fig. 2c). The upper curve in the f–v characteristics reflects force variation with decreasing velocities ($dv/dt < 0$), while the lower curve corresponds to force with increasing velocities ($dv/dt > 0$). The mean slope of the hysteretic loop, referred to as the viscous damping coefficient, is dependent upon both the control current and the excitation conditions (frequency and stroke).
5. *Viscous character.* Given a control current, the MR damper would yield nearly identical f–v curves under the same excitation velocity which may be realized from different combinations of frequency and stroke. The damping force can therefore be expressed as a function of piston velocity and control current, with appropriate consideration of the force-limiting behaviour.

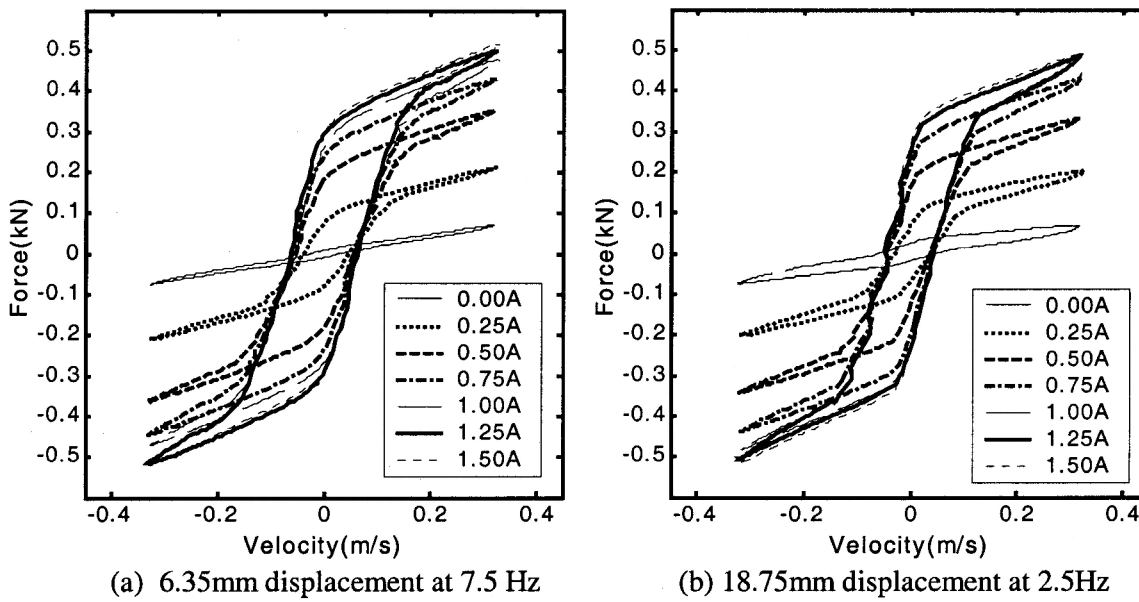

Fig. 3 Force–velocity characteristics as functions of applied current

3 MODEL SYNTHESIS

The f–v characteristics of the MR damper reveal pronounced non-linear hysteresis and force-limiting properties. Hysteresis is a widely known phenomenon commonly encountered in a broad spectrum of physical systems. Structures invariably exhibit hysteresis, especially when the response becomes inelastic [**13**, **14**]. The model synthesis of such systems thus poses a challenging task. In this study, the equivalent characteristic method (ECM) is applied on the basis of experimental data to achieve a model synthesis in the form of a non-linear algebraic function fully to characterize the hysteretic characteristics of the MR damper. The model also builds upon the observed features to enhance an understanding of the underlying damping mechanism, and relationships between the hysteresis and nature of excitation (frequency and stroke).

3.1 Generalized characteristic parameters

The typical f–v characteristics of an MR damper, corresponding to specific magnitudes of velocity and control current, can be represented by the general hysteresis loop shown in Fig. 4. The mean damping characteristics, frequently used to evaluate the overall system response [**4**, **12**], can also be easily derived from the loop, as shown by the bold curve. The model synthesis can be obtained from the generalized hysteresis loop with appropriate consideration of the features observed from the experimental data. The essential parameters required to formulate the model are described below. Owing to the symmetry, the parameters are described for compression alone ($v \geqslant 0$):

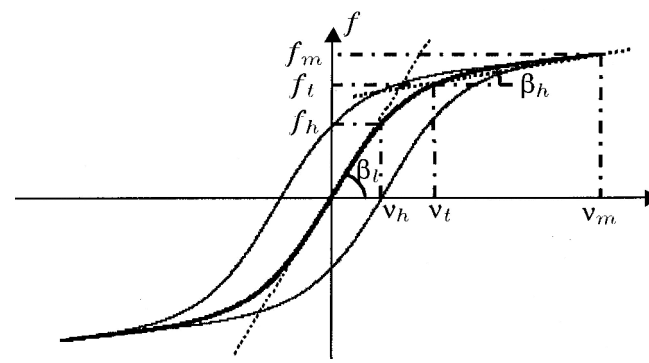

Fig. 4 Generalized hysteretic f–v characteristics

(a) maximum velocity, v_m (m/s): maximum velocity of the damper piston, determined from the excitation frequency and stroke;
(b) maximum force, f_m (N): maximum force developed by the MR damper, corresponding to specified v_m and control current i;
(c) zero-force velocity intercept, v_h (m/s): piston velocity corresponding to zero damping force under given i and excitation conditions;
(d) zero-velocity force intercept, f_h (N): damping force corresponding to zero velocity under given i and excitation condition;
(e) transition velocity, v_t (m/s): piston velocity corresponding to the onset of the force-limiting property (post-yield condition) leading to linearly increasing force and saturation, as derived from the mean curve; the transition velocity is obtained from the intersection point (f_t, v_t) of the tangent curves drawn to the mean f–v curve near $v = 0$ and to the mean curve in the post-yield (slope $= \beta_h$), as shown in Fig. 4;

(f) transition force, f_t (N): mean damping force corresponding to v_t;
(g) low-velocity slope, β_l (N s/m): slope of the mean f–v curve at $v = 0$, representing the low-speed viscous damping coefficient;
(h) high-velocity slope, β_h (N s/m): slope of the mean f–v curve at v_t, representing the high-speed viscous damping coefficient.

3.2 Synthesis of the characteristic curves

The family of f–v hysteresis curves for the MR damper (Fig. 3) is described by three distinct properties:

(a) saturated hysteresis loop,
(b) linear rise,
(c) current-induced rise.

The various curves attained at increasing control currents may be considered as an amplification of the passive characteristics ($i = 0$). A saturated hysteresis loop in the absence of linear rise, $f_s(v + v_h)$, can be formulated by the *symmetric sigmoid* function with bideflection in the lateral axis

$$f_s(v + v_h) = f_t \frac{1 - e^{-\alpha(v + v_h)}}{1 + e^{-\alpha(v + v_h)}} \quad (1)$$

where v is the instantaneous relative velocity of the damper piston and α is a constant used to adjust the slope of the hysteresis curve.

The *linear rise* segment of the curves, which relates to the force-limiting property in the post-yield condition, can be expressed by the linear function $c_v(v)$, which is often referred to as the high-velocity damping coefficient

$$c_v(v) = 1 + k_v \cdot |v| \quad (2)$$

where k_v is a constant describing the influence of excitation condition on the linear rise.

Equations (1) and (2) allow the formulation of a general hysteresis loop as shown in Fig. 5

$$f(v + v_h) = f_t \frac{1 - e^{-\alpha(v + v_h)}}{1 + e^{-\alpha(v + v_h)}} (1 + k_v \cdot |v|) \quad (3)$$

3.3 Influence of control current

If the *current-induced rise* is considered as a shift of the f–v curve, the role of control current in the model synthesis can be modelled as a gain $c_i(i)$ limiting the force to f_t. The gain function, $c_i(i)$, is derived with systematic consideration of the relationships between f_t, v_h, α and k_v corresponding to given excitation condition and control current. This requires the derivation of rather complex relationships among the various characteristic parameters (f_t, v_h, α, k_v) and excitation conditions, as described below.

3.3.1 Transition force f_t

The experimental data suggest a strong dependence of f_t on both the control current, i, and the excitation condition, v_m. The transition force may thus be expressed as

$$f_t = f_0 c_e c_i \quad (4)$$

where f_0 denotes the constant base value of f_t taken as the seal friction force, while coefficients c_e and c_i describe the influence of v_m and i on f_t respectively. This is evident from the variation in the measured transition force as a function of v_m and i, as shown in Fig. 5. The results also show the non-linear incremental behaviour that can be characterized by an *asymmetric sigmoid function* with a

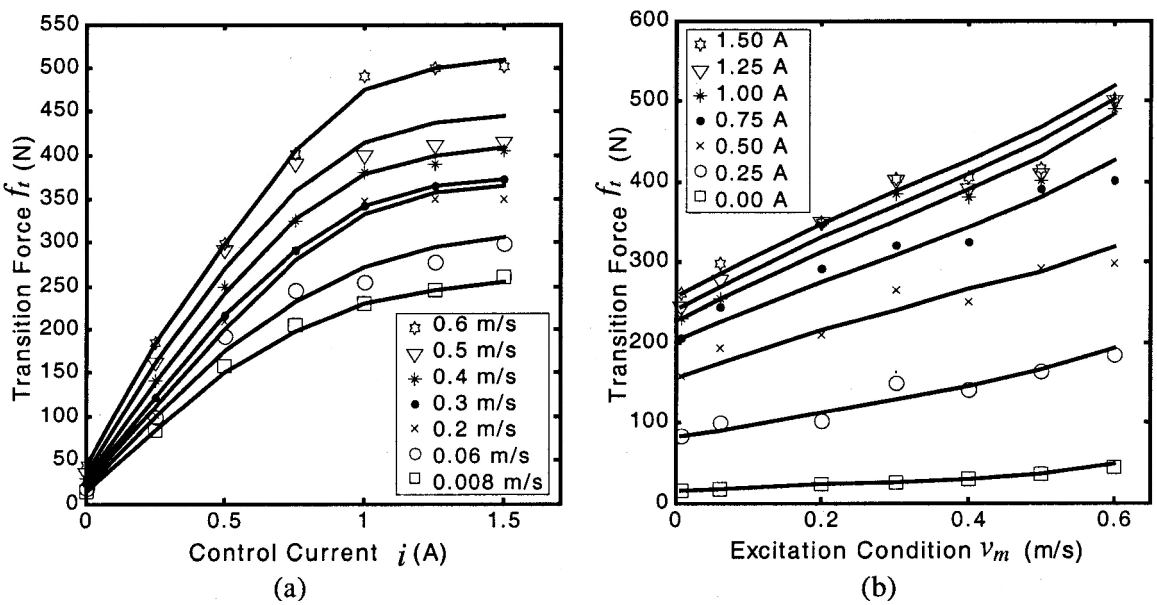

Fig. 5 Measured transition force f_t as a function of i and v_m

certain bias in the lateral axis. Consequently, the control current gain, c_i, is expressed as

$$c_i(i) = 1 + \frac{k_2}{1 + e^{-a_2(i+I_0)}} - \frac{k_2}{1 + e^{-a_2 I_0}} \tag{5}$$

where k_2 and a_2 are positive constants, and I_0 is an arbitrary constant. Equation (5) yields a unit value of c_i for a passive damper ($i = 0$).

The evolution of f_t in relation to v_m with varying control current i can also be observed from the measured data plotted in Fig. 5b. The data suggest that f_t can be expressed by an exponential function of v_m. The coefficient c_e is thus formulated as

$$c_e(v_m) = 1 + e^{a_1 v_m} \tag{6}$$

where a_1 is a positive constant used to adjust the rising rate of the exponent v_m. It should be noted that the maximum velocity, v_m, is not a directly measurable quantity. It is, however, essential to derive a relationship between the hysteretic characteristics and v_m, which would enhance the synthesis for implementation over a broad range of operating conditions. The measured data (Figs 2 and 3) clearly show that the damper response is strongly dependent upon excitation frequency, ω, and stroke, a_m. Although these excitation conditions can be equivalently expressed by the maximum velocity for harmonic motion, $v_m = \omega a_m$, v_m cannot be directly measured in real time, specifically under random excitations. Alternatively, the magnitude of v_m can be derived from the instantaneous position, x, and acceleration, $\ddot{x}$

$$v_m = a_m \omega = \sqrt{(\dot{x})^2 - \ddot{x} \cdot x} \tag{7}$$

where $\dot{x} = v$ and $\ddot{x} = dv/dt$ are the instantaneous piston velocity and acceleration respectively.

Substituting c_i and c_e from equations (5) and (6) into (4), the transition force f_t may be expressed as

$$f_t = f_0(1 + e^{a_1 v_m})\left(1 + \frac{k_2}{1 + e^{-a_2(i+I_0)}} - \frac{k_2}{1 + e^{-a_2 I_0}}\right) \tag{8}$$

3.3.2 *Linear rise coefficient k_v*

The rate of linear rise at high velocities, β_h, can be estimated from the mean f–v curve, as shown in Fig. 4

$$\beta_h = \frac{f_m - f_t}{v_m - v_t} \tag{9}$$

where the parameters f_m, f_t, v_m and v_t are characteristic parameters deduced from the measured data corresponding to different values of current i. Equation (9) is solved to calculate the slope of the high-velocity region as a function of v_m and i. Figure 6 further shows the dependence of β_h on v_m and i, as derived from the measured data. The results show exponential decay in β_h with increasing v_m under a constant control current i, and a gradual increase with i under a specified v_m. The identical trends are also evident from the computed results presented in Table 1.

The effect of i on β_h can be further obtained from analysis of the general formulation of the hysteresis model described in equation (3). Owing to the saturation property of the sigmoid function, the rate of change in force with respect to velocity corresponding to higher velocities yields the following relationship between β_h and the linear rise coefficient k_v

$$\beta_h = f_t k_v = f_0 c_e c_i k_v \tag{10}$$

The above relation reveals that β_h depends on both the excitation condition v_m and the control current i. The measured data presented in Fig. 6 further suggest that

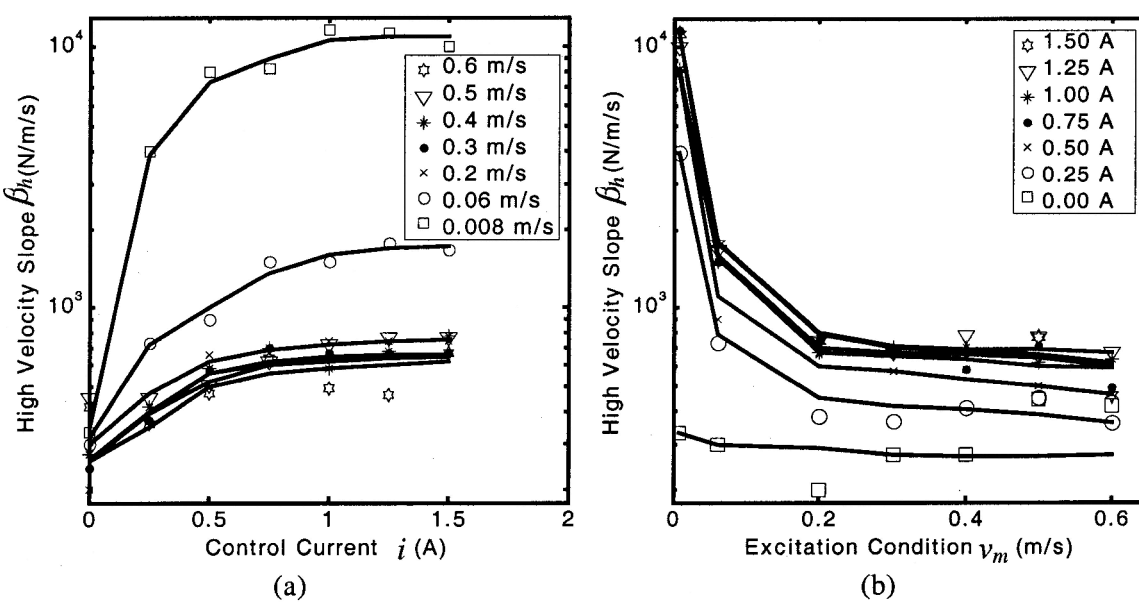

Fig. 6 Variations in high-velocity slope β_h with i and v_m

Table 1 High-velocity slope β_h as a function of v_m and i

	High-velocity slope β_h (N s/m)						
i (A)	$v_m =$ 0.008 m/s	$v_m =$ 0.06 m/s	$v_m =$ 0.2 m/s	$v_m =$ 0.3 m/s	$v_m =$ 0.4 m/s	$v_m =$ 0.5 m/s	$v_m =$ 0.6 m/s
0.00	333	300	200	274	274	445	417
0.25	4000	733	384	367	414	450	360
0.50	8000	900	657	573	580	497	467
0.75	8333	1500	670	700	700	617	637
1.00	11 667	1500	744	667	580	717	490
1.25	11 333	1767	744	667	680	767	460
1.50	10 000	1667	744	668	772	767	667

the excitation condition has a relatively small effect at higher velocities. Considering that the coefficient c_e increases exponentially with v_m, the linear rise coefficient, k_v, can be expressed as

$$k_v = k_1 \, e^{-a_4 v_m} \tag{11}$$

where k_1 and a_4 are positive constants.

3.3.3 *Hysteresis slope coefficient* α

The low-velocity slope β_l of the hysteretic loop, shown in Fig. 4, can be derived from the characteristic parameters f_h and v_h as $\beta_l = f_h/v_h$. Table 2 summarizes the slope values for different values of v_m and i. Figure 7 further illustrates the variations in β_l with v_m and i, as derived from the measured data under selected excitation conditions. The results show trends identical to those observed for the high-velocity slope in Fig. 6, namely a rapidly decaying β_l with increasing v_m.

The low-speed slope could also be calculated from equation (3) by taking the rate of change in force with respect to velocity corresponding to $v = 0$, such that

$$\beta_l = \tfrac{1}{2}\alpha f_t = \tfrac{1}{2}\alpha f_0 c_e c_i \tag{12}$$

Considering that the coefficient c_e increases exponentially with v_m, the hysteresis slope coefficient α can be expressed as

$$\alpha = \frac{a_0}{1 + k_0 v_m} \tag{13}$$

where a_0 and k_0 are positive constants of the decreasing function α.

3.3.4 *Zero-force velocity intercept* v_h

The zero-force velocity intercept v_h, shown in Fig. 4, strongly affects the shape of the hysteresis curve, specifically the width of the hysteretic loop. The variations in v_h with v_m for different values of i and variations in v_h with i for different values of v_m were deduced from the measured data (Fig. 8). The results show a strong dependence of v_h not only on the excitation condition v_m but also on the control current i. The dependence of v_h on i for given values of v_m can be formulated by an asymmetric function similar to that defined for $c_i(i)$ in equation (5). The dependence of v_h on v_m for given values of i can be described as a linear function of v_m. Furthermore, the sign of v_h can be determined from $\text{sign}(dv/dt)$. For $dv/dt = 0$, the velocity v approaches its maximum value v_m, and the two enveloping curves converge. The zero-force velocity intercept can thus be expressed as a function of v_m and i in the following manner:

$$v_h = \text{sign}(\ddot{x}) k_4 v_m \left(1 + \frac{k_3}{1 + e^{-a_3(i + I_1)}} - \frac{k_3}{1 + e^{-a_3 I_1}} \right) \tag{14}$$

where a_3, k_3, k_4 and I_1 are positive constants.

3.4 Synthesis of the overall model

The overall model synthesis can be established from the generalized hysteresis loop model [equation (3)] by integrating the above formulations describing the non-linear

Table 2 Low-velocity slope β_l as a function of v_m and i

	Low-velocity slope β_l (N s/m)						
i (A)	$v_m =$ 0.008 m/s	$v_m =$ 0.06 m/s	$v_m =$ 0.2 m/s	$v_m =$ 0.3 m/s	$v_m =$ 0.4 m/s	$v_m =$ 0.5 m/s	$v_m =$ 0.6 m/s
0.00	7692	3000	1429	550	485	372	216
0.25	36 250	8720	2270	2010	1500	1240	1000
0.50	47 429	10 200	4760	3750	2280	1867	1530
0.75	68 205	14 837	6230	4033	2860	2463	1904
1.00	74 286	14 810	6710	4453	2990	2442	2232
1.25	80 909	14 570	6464	4485	3590	2518	2236
1.50	81 333	14 500	6110	7222	3822	2600	2340

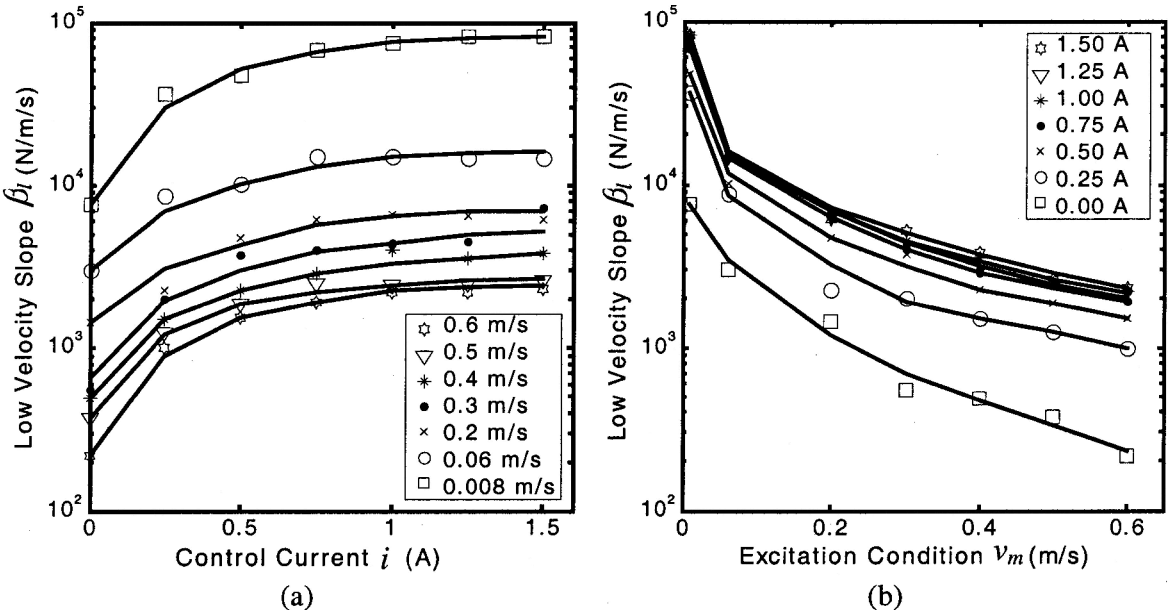

Fig. 7 Variations in low-velocity slope β_l with i and v_m

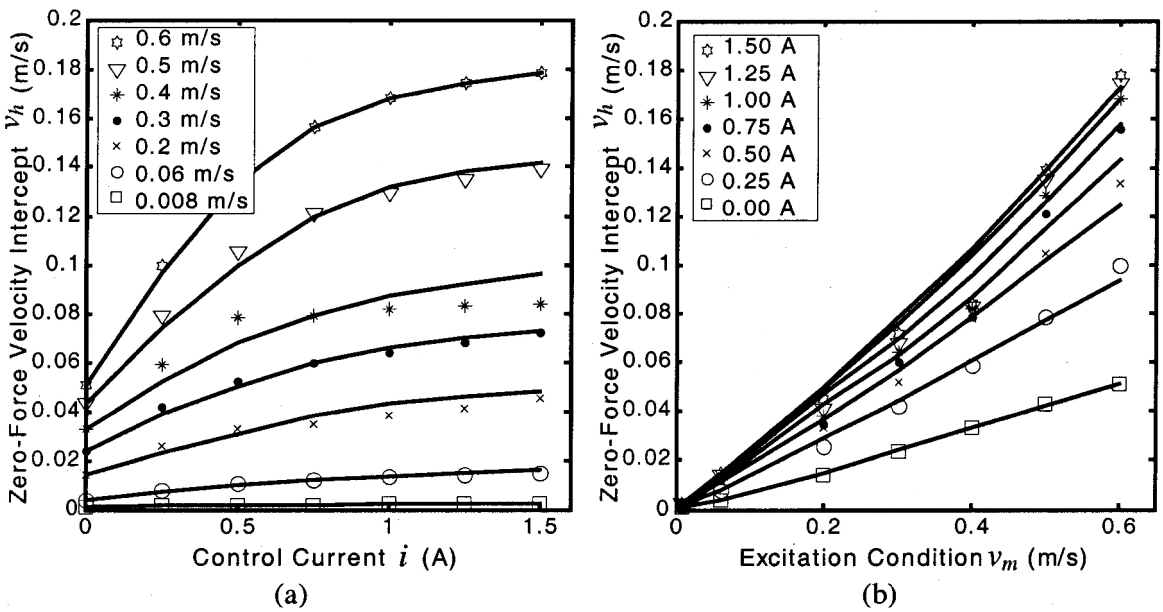

Fig. 8 Variations in zero-force velocity intercept v_h with i and v_m

dependence of force on control current

$$f(v, i) = f_t(i)\frac{1 - e^{-\alpha(v+v_h)}}{1 + e^{-\alpha(v+v_h)}}(1 + k_v \cdot |v|) \tag{15}$$

The current- and excitation-dependent functions that were formulated in the above section are summarized below

$$f_t(i) = f_0(1 + e^{a_1 v_m})\left(1 + \frac{k_2}{1 + e^{-a_2(i+I_0)}} - \frac{k_2}{1 + e^{-a_2 I_0}}\right)$$

$$v_h = \text{sign}(\ddot{x}) k_4 v_m \left(1 + \frac{k_3}{1 + e^{-a_3(i+I_1)}} - \frac{k_3}{1 + e^{-a_3 I_1}}\right)$$

$$\alpha = \frac{a_0}{1 + k_0 v_m}, \qquad k_v = k_1 e^{-a_4 v_m},$$

$$v_m = \sqrt{(\dot{x})^2 - \ddot{x} \cdot x}$$

The overall model requires identification of a total of 13 parameters (f_0, I_0, I_1, a_0, a_1, a_2, a_3, a_4, k_0, k_1, k_2, k_3 and k_4) from the measured data. It should be noted that the above hysteretic model can be easily simplified to the mean f–v model by letting $k_4 = 0$ (i.e. $v_h = 0$), and the number of parameters to be identified can be reduced from 13 to 10. The measured data acquired under a wide range of excitation conditions and control current have

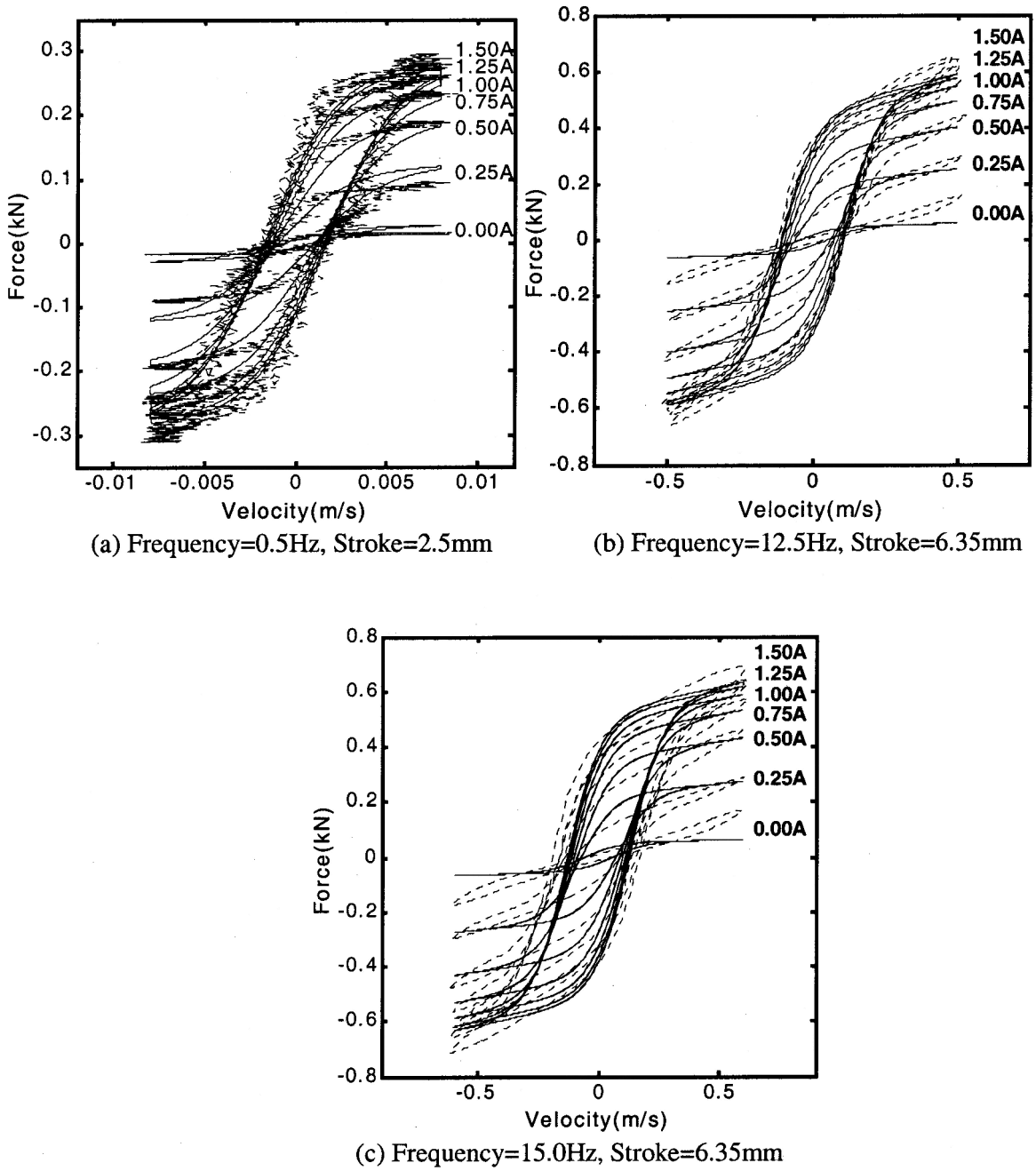

Fig. 9 Comparison of simulation results with the measured data under different operating conditions

been thoroughly analysed to identify the model parameters for the particular damper considered and are summarized in Table 3.

Table 3 Model parameters identified from the measured data

Parameter	Value	Parameter	Value
a_0	990	k_0	112.5
a_1 [(m/s)$^{-1}$]	1.75	k_1	5.55
a_2 (A^{-1})	2.85	k_2	19.4
a_3 (A^{-1})	1.55	k_3	2.90
a_4 [(m/s)$^{-1}$]	4.60	k_4	0.095
I_0 (A)	0.05	f_0 (N)	13.9
I_1 (A)	−0.08		

4 MODEL VALIDATION

The proposed model synthesis [equation (15)] has been analysed under a wide range of excitation conditions (stroke and frequency) and control current. The simulation results are compared with the measured data to evaluate the effectiveness of the model. The comparisons show reasonably good agreement between the simulation

results and the test data, over the entire range of test conditions considered, with the exception of those attained under low levels of command current. Figures 9 and 10 compare simulation results in terms of force–velocity characteristics with measured data under a number of test conditions, as examples, to demonstrate the validity of the proposed model. The results also show the force–displacement response under 6.35 mm excitation at 7.5 Hz. Comparison of the f–d curves attained from simulation and measured data under different values of control current show similar degrees of agreement. Figure 11 compares simulation results with measured data under different excitation frequencies and velocities, corresponding to $i = 0.75$ A. The results show similar degrees of agreement in the entire range of frequencies and peak velocities considered in the study.

The effectiveness of the synthesized model is further investigated through simulation performed with an arbitrary complex harmonic piston displacement signal composed of three harmonics with frequencies of 0.5, 2.5 and 5.0 Hz and respective amplitudes of 6.35, 12.5 and 12.5 mm. The control current is also varied using a multistep signal with amplitudes of 0.0, 0.25, 1.5, 0.5 and 0.0 A, while the time duration of each step is limited to 1 s. It should be noted that this control current also represents the coil current, as stated earlier. Equation (15) is solved to derive the damping force developed by the MR damper model under prescribed displacement

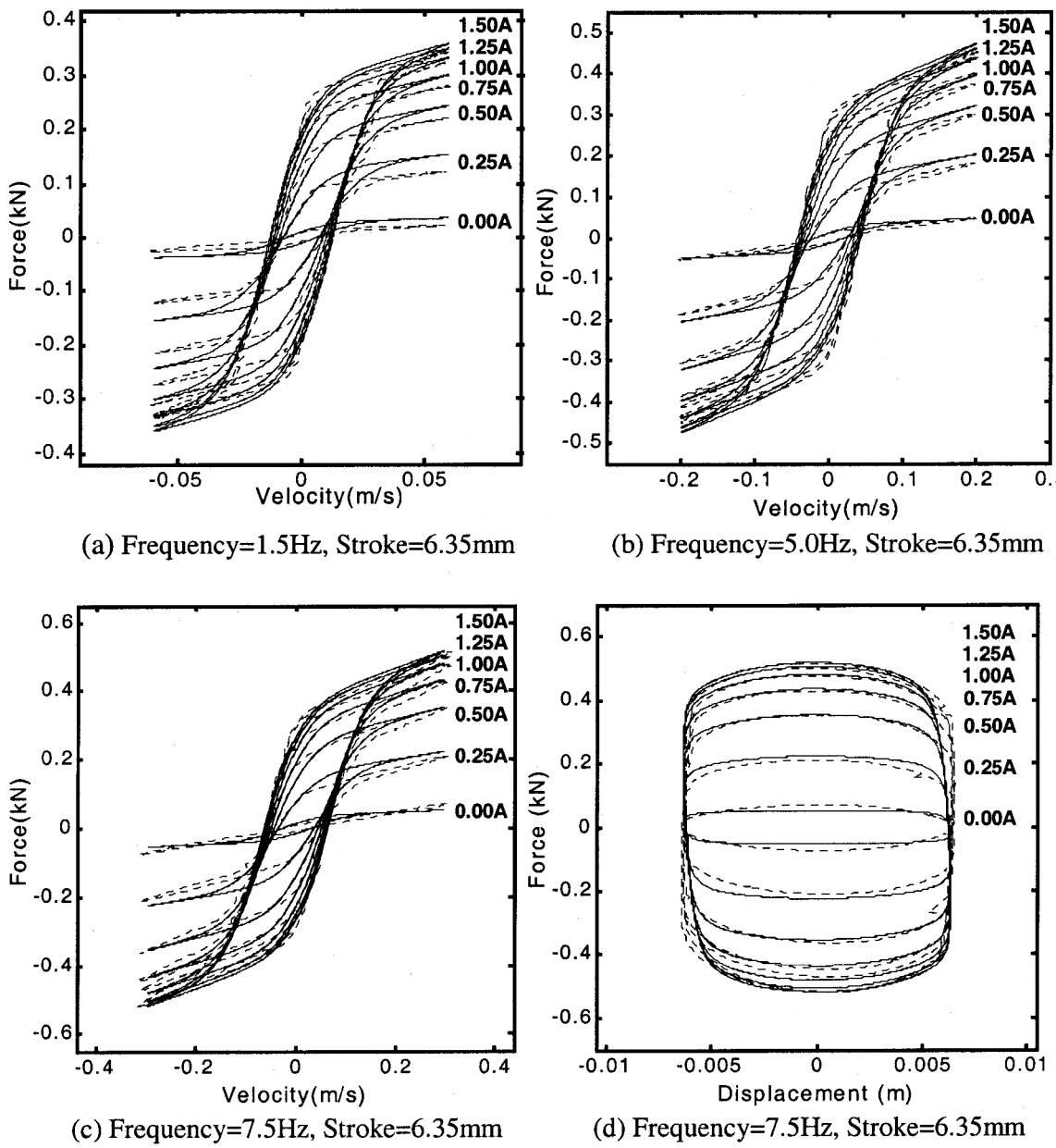

Fig. 10 Comparison of simulation results with the measured data under different operating frequencies

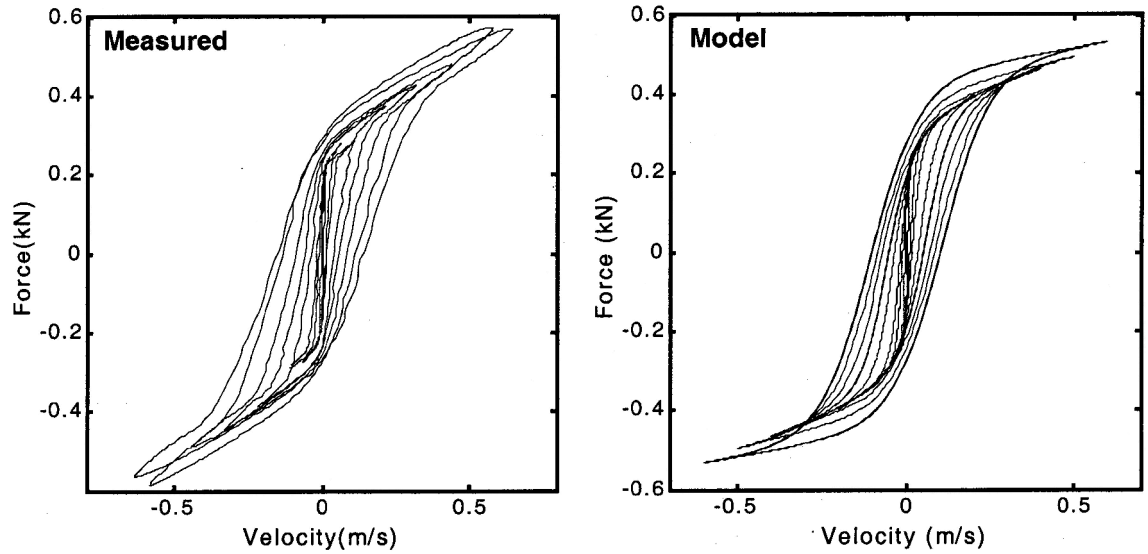

(a) Stroke=6.35mm; Current=0.75A; Frequencies are 15.0 Hz, 12.5 Hz, 10.0 Hz, 7.5 Hz, 5.0 Hz, 2.5 Hz, 1.5 Hz, 0.5 Hz, from the outside loop to the inside loop;

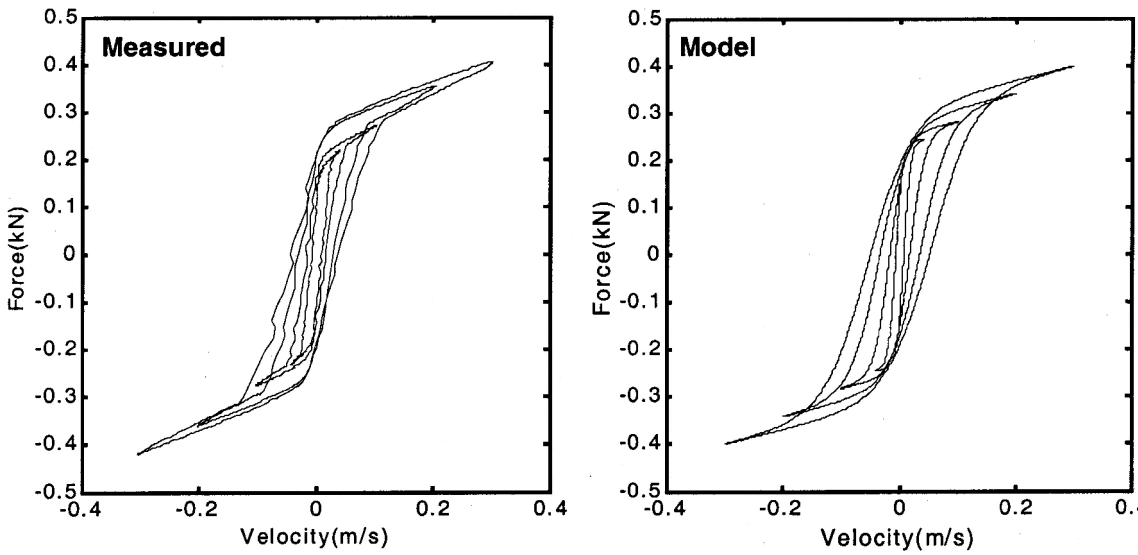

(b) Frequency=2.5Hz; Current=0.75A; Strokes are 18.75mm, 12.5mm, 6.35mm, 2.54mm, from the outside loop to the inside loop

Fig. 11 Comparison of simulation and experimental results: (a) response with different excitation frequencies; (b) response with varying excitation amplitudes

excitation and control current. Figure 12 shows the damping force response, together with the excitation and command current signals. The results show a strong correlation between the peak damping force and the magnitude of command current and displacement excitation.

5 CONCLUSIONS

A generalized model synthesis is proposed to characterize the hysteretic force–velocity characteristics of a controllable MR damper under a wide range of sinusoidal excitation conditions (frequency and displacement amplitude) and magnitudes of control current. The essential features of the model are derived on the basis of measured force–displacement, force–velocity and seal friction properties of an MR damper attained under a wide range of excitation conditions. The model formulation is systematically realized on the basis of the fundamental force generation mechanism and observed qualitative trends of the measured data. The global model synthesis is realized by integrating the components describing the excitation- and current-dependent hysteretic linear rise in the preyield

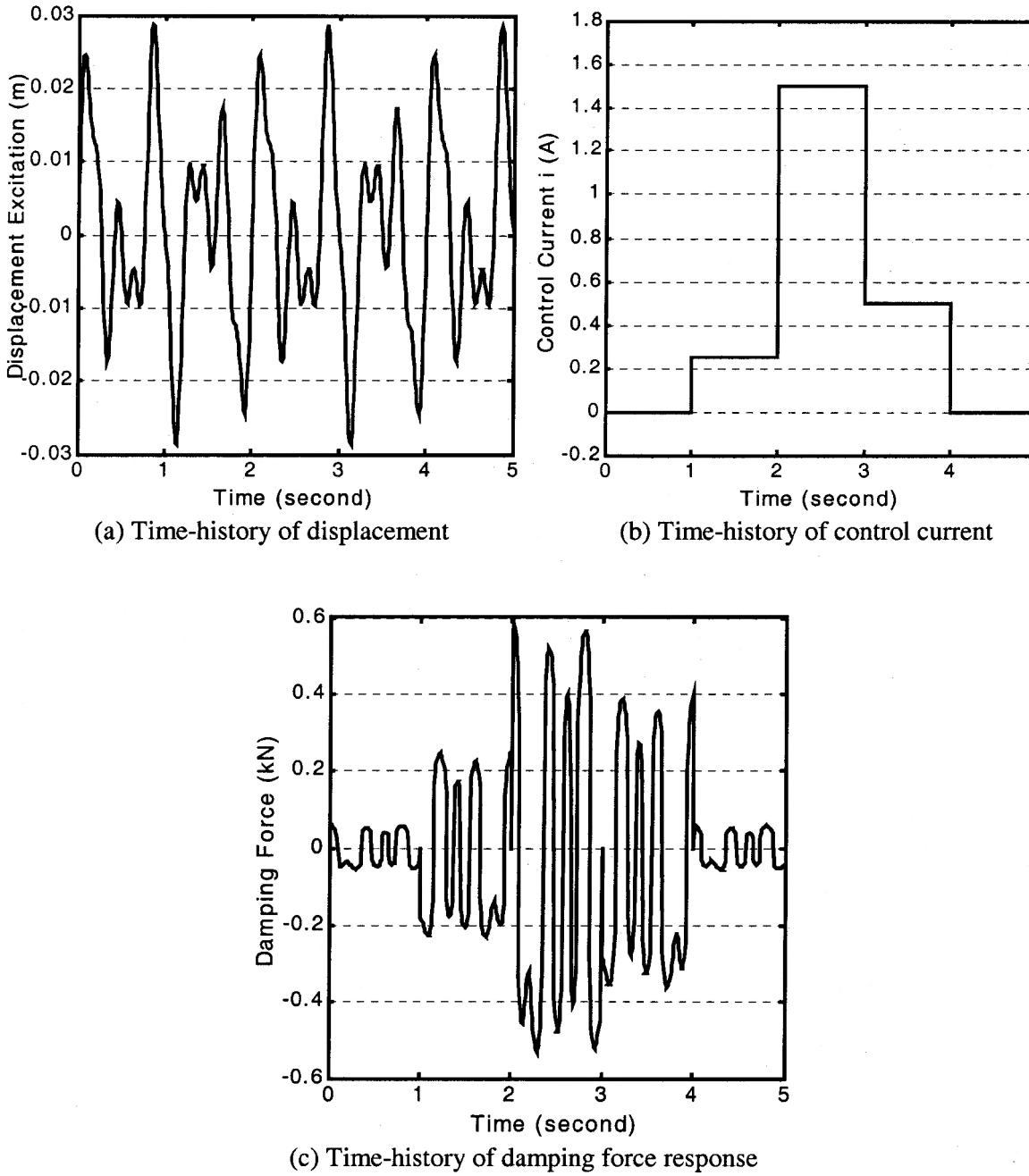

Fig. 12 Simulation results attained under an arbitrary displacement excitation and control current

condition, force limiting in the post-yield condition, the zero-force velocity intercept, the zero-velocity force intercept and the yield force corresponding to the onset of saturation. Simulations are performed to assess the effectiveness of the proposed model synthesis, and results obtained under a wide range of simulation conditions are compared with those obtained from the measured data. The results show reasonably good agreement between the simulation results and the measured data, irrespective of the excitation conditions and control current. It is thus concluded that the proposed model can effectively describe the non-linear steady state hysteretic dynamic properties of the controllable MR damper and can thus be effectively used to design an optimal semi-active controller for implementation in vehicle suspension.

ACKNOWLEDGEMENTS

This work was supported by the Chinese Scholarship Council (CSC), the Fellowship of Concordia University and the Lord Cooperation (United States).

REFERENCES

1 **Choi, S. B., Lee, B. K., Nam, M. H.** and **Cheong, C. C.** Vibration control of a MR seat damper for commercial vehicles. Smart Structures and Materials 2000: Smart Structures and Integrated Systems. *Proc. SPIE*, 2000, **3985**, pp. 491–496.

2 **Choi, S. B., Lee, H. S., Hong, S. R.** and **Cheong, C. C.** Control and response characteristics of a magneto-rheological fluid damper for passenger vehicles. Smart Structures and Materials 2000: Smart Structures and Integrated Systems. *Proc. SPIE*, 2000, **3985**, pp. 438–443.

3 **McManus, S. J., StClair, K. A., Boileau, P. É., Rakheja, S.** and **Boutin, J.** Evaluation of vibration and shock attenuation performance of a suspension seat with semi-active magneto-rheological fluid damper. *J. Sound and Vibr.*, 2002, **253**(1), 313–327.

4 **Milliken, W. F.** and **Milliken, D. L.** *Race Car Vehicle Dynamics*, 1995 (Society of Automotive Engineers).

5 **Carlson, J. D.** and **Sproston, J. L.** Controllable fluids in 2000—status of ER and MR fluid technology. Actuator 2000, 7th International Conference on *New Actuator*, Bermen, Germany, 19–21 June 2000, pp. 126–130.

6 **Carlson, J. D.** Implementation of semi-active control using magnetorheological fluids. Mechatronic System, Proceedings Volume from IFAC Conference 2000, Germany, 2000, pp. 973–978.

7 **Wereley, N. M., Pang, L.** and **Kamath, G. M.** Idealized hysteresis modeling of electro-rheological and magneto-rheological dampers. *J. Intell. Mater. Syst. and Struct.*, 1998, **9**, 642–649.

8 **Spencer Jr, B. F., Dyke, S. J., Sain, M. K.** and **Carlson, J. D.** Phenomenological model for a magneto-rheological damper. *J. Engng Mechanics, Am. Soc. Civil Engrs*, 1997, **123**, 230–238.

9 **Choi, S. B.** and **Lee, S. K.** A hysteresis model for the field-dependent damping force of a magneto-rheological damper. *J. Sound and Vibr.*, 1997, **245**(2), 375–383.

10 **Dyke, S. J., Spencer Jr, B. F., Sain, M. K.** and **Carlson, J. D.** Seismic response reduction using magneto-rheological dampers. In Proceedings of 13th IFAC Triennial World Congress, 1996, pp. 145–150.

11 **Stanway, R., Sproston, J. L.** and **El-Wahed, A. K.** Application of electrorheological fluids in vibration control: a survey. *Smart Mater. and Struct.*, 1996, **5**(4), 464–482.

12 **Warner, B.** An analytic and experimental investigation of high performance suspension dampers. PhD dissertation, Corcordia University, Canada, 1996.

13 **Wen, Y. K.** Method for random vibration of hysteretic systems. *J. Engng Mechanics Div.*, 1976, **102**, 249–263.

14 **Nakano, M., Yamamoto, H.** and **Jolly, M. R.** Dynamic viscoelasticity of a magneto-rheological fluid in oscillatory slit flow. *Int. J. Mod. Phys.*, 1999, **B**(13), 2068–2076.